American Journal of Innovation in Science and Engineering (AJISE)

ISSN: 2158-7205 (ONLINE)

VOLUME 4 ISSUE 3 (2025)

PUBLISHED BY
E-PALLI PUBLISHERS, DELAWARE, USA

American Journal of Innovation in Science and Engineering (AJISE)

Volume 4 Issue 3, Year 2025
ISSN: 2158-7205 (Online)
DOI: https://doi.org/10.54536/ajise.v4i3.5889
https://journals.e-palli.com/home/index.php/ajise

Management of Voltage Profile and Minimization of Power Losses in a Distribution Network with Embedded Wind Energy Conversion System using GOA-Tuned SMES Unit

Steven Sesay[1*], Cyrus Wabuge Wekesa[1]

Article Information

Received: August 23, 2025
Accepted: September 28, 2025
Published: December 18, 2025

Keywords

Current Source Converter-Superconducting Magnetic Energy Storage Unit, Distribution Network, Double Fed Induction Generator, Grasshopper Optimization Algorithm

ABSTRACT

Distribution networks are prone to voltage fluctuations and power losses due to line impedances, variable renewable energy generation, network configuration, and sudden changes in load. Superconducting Magnetic Energy Storage (SMES) unit has demonstrated capability to tackle these problems. This paper investigates a Grasshopper Optimization Algorithm (GOA) tuned Current Source Converter (CSC)-SMES in a distribution network with an embedded Wind Energy Conversion System (WECS) to manage voltage profiles and minimize power losses. The system was modeled in MATLAB/Simulink and tested under incremental load increases in a state of discharge condition. Comparative analysis between a conventional PI controlled SMES and a GOA-tuned SMES revealed superior performance with optimization based tuning. For a 15% load increase, the conventional controller (K_p = 1.47 K_i= 0.76) yielded a Voltage Profile Improvement Index (VPII) of 1.011, real power loss of 0.264 p.u., and reactive power loss of 0.211 p.u. The GOA-tuned controller (K_p = 1.66, K_i = 0.95) achieved a VPII of 1.014, reducing real and reactive power losses to 0.257 p.u. and 0.204 p.u., respectively, corresponding to 2.15% and 4.16% improvements. The results confirm that GOA tuned SMES controller performance, providing improved voltage stability and reduced losses in distribution networks integrated with wind energy source.

INTRODUCTION

Overloaded distribution networks lead to elevated energy costs, recurring power outages, degraded power quality, and reduced reliability worldwide (Burke & Stephens, 2018). Electricity demand has risen sharply today, whereas fossil fuel use and investments in supporting power system infrastructure have significantly decreased. Traditional power distribution systems follow a rigid hierarchical structure. Furthermore, power systems are increasingly shifting toward Distributed Energy Resources (DERs), driven by factors such as rising energy demand, rapid technological progress, fuel shortages, outages, financial supports, and increasing societal consciousness about ecological issues. These DER-based networks offer enhanced reliability, stability, quality, and security. Currently, DERs have become a standard feature in many utilities across the globe. In practice, these energy sources are now being more widely incorporated into distribution networks. The integration of these energy sources has proven vital for distribution networks, as they help reduce power losses, enhance system voltage levels, and serve as environmentally friendly green energy solutions (Said *et al.,* 2018). The reliability of a distribution network can be affected by renewable sources like wind power, given their variability and dependence on weather conditions. Rising load demand in distribution networks can lead to greater voltage drops, negatively affecting power losses, voltage profiles, and overall system stability. To mitigate these challenges and provide additional benefits, distribution networks are increasingly adopting Energy Storage Systems (ESS). These consist of flywheel storage (Yakout *et al.,* 2021), fuel cell storage (Buckles & Hassenzahl, 2000), compressed air energy storage (Luo *et al.,* 2014), compressed carbon dioxide energy storage (Chaychizadeh *et al.,* 2018), battery energy storage system (Sadiq *et al.,* 2021) , and Superconducting Magnetic Energy Storage (SMES) (Qais *et al.,* 2020). SMES has proven to be crucial for incorporating renewable energy sources, like wind power plants, into power systems (Nielsen & Molinas, 2010).

SMES unit comprises three main elements: cryogenic refrigerator, Power Conditioning System (PCS), and superconducting coil. In comparison with other energy storage systems (ESS), SMES offers distinct advantages, including faster response time, higher efficiency, and extended operational lifespan. Energy storage is achieved through the magnetic field generated by a sizable superconducting coil, which cooled to a temperature below its superconducting critical point (Wong *et al.,* 2019). The coil, which may be designed as either a solenoid or toroid, serves as the core element of the SMES unit (Wong *et al.,* 2019; Mahlia *et al.,* 2014). The PCS facilitates both charging and discharging operations of the superconducting coil. The two primary PCS configurations widely used are the Current Source Converter (CSC) and the Voltage Source Converter (VSC) (Wong *et al.,* 2019), where the VSC usually consists of a DC chopper and an inverter forming a two stage circuit, whereas the CSC operates as a single stage circuit. Compared to VSC-SMES, CSC-SMES offers several advantages, including a simpler structure,

[1] Department of Electrical Engineering, Pan African University Institute for Basic Science, Technology and Innovation, Nairobi, Kenya
[*] Corresponding author's e-mail: stevensesay89@gmail.com

faster dynamic response, lower implementation cost, and ease of control (Xing *et al.,* 2016). Nonetheless, both PCS configurations are capable of injecting or absorbing real and reactive power, thereby mitigating key operational challenges associated with Wind Energy Conversion Systems (WECS) (Mukherjee & Rao, 2019).

The efficiency of SMES largely depends on the control method adopted for the PCS. The conventional Proportional Integral (PI) controller is widely employed in both CSC and VSC SMES systems. However, its effectiveness diminishes under sudden load variations and fluctuations in wind power. Recent advancements in artificial intelligence have motivated the use of optimization algorithms to fine tune controller parameters, enabling PI controllers to perform more reliably under diverse operating conditions (Muisyo *et al.,* 2022). In this context, the GOA has been explored for tuning CSC-SMES controllers. The proposed GOA-based tuning approach demonstrates improved performance by reducing real and reactive power losses while enhancing voltage stability in the test distribution system

LITERATURE REVIEW

Several approaches have been suggested for controlling voltage in distribution systems. One such method, discussed in (Paserba *et al.,* 2017), involves incorporating a STATCOM at a distribution substation. It was employed and synchronized to enhance voltage stability and minimize the rate of switching operations for On load Tap Changer (OLTC) and capacitors. To enhance the functionality of the capacitor controller and voltage regulator in a distribution substation, a supervisory control approach was proposed (Borozan *et al.,* 2001). Haque and Najafi (2005), a fuzzy dynamic programming technique was introduced to determine the optimal schedule for dispatching OLTCs and capacitors, subject to constraints on their switching operations.

Renewable energy sources like wind power exhibit intermittent characteristics, leading to voltage fluctuations due to their output power variability. The incorporation of energy resources, for example, wind energy, into the distribution network has the potential to greatly affect the voltage deviation or profile and the network's real and reactive power losses (Su, 2010). Because of the comparatively sluggish response of OLTC and voltage regulators (VR), they are incapable of addressing voltage deviations effectively (Ziadi & Abdel-Akher, 2014). In recent times, various control strategies have emerged to mitigate voltage deviation issues (Wang *et al.,* 2008). These strategies incorporate the utilization of reactive power controllers, like supplementary reactive power compensations, or reactive power management of distributed generation (Calderaro *et al.,* 2014; El Moursi *et al.,* 2014).

Various control methods have been investigated in the control of SMES to improve performance in power systems, few of these methods are briefly discussed in this subsection. Reference (Said *et al.,* 2019) investigates the impact of SMES in reducing voltage sags or swells in distribution networks with WECS integration. The study employs VSC - SMES. A Fuzzy Logic Controller (FLC) is utilized for the dc-dc chopper to regulate power transfer between the grid and the SMES coil. It has been developed to allow the SMES to either absorb or supply real power to or from the distribution network. Additionally, reactive power can be either injected or absorbed based on the voltage difference between the SMES and the DC link. Reference (Said *et al.,* 2018) examines the influence of WECS and SMES on enhancing the voltage profile of a three phase distribution network. Squirrel Cage Induction Generator and a FLC controlled VSC-SMES are used in the investigation. Results indicate that by integrating SMES with WECS at the same node in the distribution network, the voltage profile of the network can be improved. In (Aly *et al.,* 2017), a VSC-SMES is employed to minimize frequency and voltage variations in a 33-node standalone microgrid, which relies on variable power generation from renewable energy sources. It was observed that the VSC-SMES was employed to stabilize the voltage fluctuation. Reference (Abdelbadie *et al.,* 2022) presented a novel optimization technique known as the Archimedes Optimization Algorithm (AOA), which improves the stability of a WECS when integrated with a VSC-SMES employing a PI controller. Simulation findings demonstrate the efficacy of the optimally controlled SMES employing AOA in mitigating output power fluctuations and enhancing system stability, particularly during fault conditions.

It is worth knowing that the level of optimality and robustness required for the controller of SMES is primarily determined by its intended application (Adetokun *et al.,* 2022). From the literature review, it was noted that there have been no studies analysing the impact of SMES on distribution networks for active and reactive power losses and voltage profile simultaneously. With the advancement of artificial intelligence based technologies, there is a growing trend towards utilizing optimization algorithms to fine-tune and optimize controller parameters. Researchers have proposed an adaptive PI controller, where its parameters are adjusted using metaheuristic optimization algorithms (Liu *et al.,* 2004; Hasanien & Muyeen, 2015) for VSC-SMES. Therefore, this study aims to enhance the performance of distribution networks with Embedded WECS using CSC-SMES tuned by the GOA. It is recognized that as per the "No Free Lunch Theorem," no optimization technique is universally effective for every class of optimization challenges(Wolpert & Macready, 1997). To the best of our knowledge, GOA has not been applied to tuned CSC-SMES for improvement of voltage profile and minimization real and reactive power losses in distribution networks.

The Distribution Network Performance Criteria

The performance criteria considered in the study are Voltage Profile Improvement Index(VPII), and real and

reactive power losses index. These criteria are explained in the subsection as follows:

Voltage Profile Improvement Index

With the appropriate integration of SMES, an improvement in voltage profile can be observed in a network. So, Voltage Profile Improvement Index (VPII) is a major criterion considered in the optimal placement of SMES. In this research, the voltage profile of the ith node of the network (VP_i) is defined in equation 1 (Sannigrahi *et al.,* 2019).

$$VP_i=((V_i-V^{min})\times(V^{max}-V_i))/((V^{nom}-V^{min})\times(V^{max}-V^{nom})) \quad ...(1)$$

The ith node's voltage profile is denoted as V_i, considers a nominal node voltage,V^{nom} as 1. The allowable voltage limits are defined as 0.95 p.u for V^{min} and 1.05 p.u for V^{max}. The system's overall network Voltage Profile Index (VPI) is expressed in equation 2

$$VPI = 1/\tilde{N} \sum^{N}_{i=1} VP_i \quad ....(2)$$

where $\tilde{N}$ is the total load nodes number. Thus, the netw ork's VPII can be determined using equation 3.

$$VPII = (VPI_{with\ smes})/(VPI_{without\ smes}) \quad ....(3)$$

If the VPII falls below 1, it suggests that the inclusion of the SMES exacerbates the network voltage profile. Conversely, if the VPII exceeds 1, it indicates an improvement in the network voltage due to the SMES. If the VPII remains at unity, it implies that the SMES does not affect the network voltage. A higher VPII value signifies a greater improvement in the voltage profile (Sannigrahi *et al.,* 2019) within the specified voltage limit.

Power Loss Index

SMES serve a crucial role in reducing the real and reactive power losses of a network which can be expressed in percentage. Thus, ΔP_{Loss} and ΔQ_{Loss} in percentage, is recognized as performance criteria in this research. Equations (4) and (5) are used to determine ΔP_{Loss} and ΔQ_{Loss} , respectively.

$$\Delta P_{Loss}=(((P_{Loss})_{with\_smes}-(P_{Loss})_{without\_smes})/(P_{Loss})_{without\_smes})\times 100 \quad ....(4)$$

$$\Delta Q_{Loss}=((Q_{Loss})_{with\_smes}-(Q_{Loss})_{without\_smes})/(Q_{Loss})_{without\_smes}\times 100 \quad ....(5)$$

where P_{Loss} is the real power loss, Q_{Loss} represent the reactive power loss. ΔP_{Loss} and ΔQ_{Loss} represent the percentage decrease in real and reactive power losses, respectively.

Grasshopper Optimization Algorithm

Mirjalili *et al.* (2018) introduced the GOA, is a novel and intriguing swarm intelligence system that simulates the foraging and swarming behaviors of grasshoppers (Meraihi *et al.,* 2021). GOA exhibits high accuracy and achieves excellent solutions, surpassing established and contemporary algorithms in the literature (Saremi *et al.,* 2017). Previous research simulations have shown that the GOA-based algorithm yields better results compared to other metaheuristic algorithms like GA and PSO (Kumar *et al.,* 2022; Mirjalili *et al.,* 2018). Each grasshopper within the swarm possesses a unique position, offering a possible approach to solving the optimization problem. The position of the ith grasshopper, denoted as X_j , is determined by equation 6 (Sajjad *et al.,* 2023).

$$X_j = \alpha_j + \beta_j + \gamma_j \quad ....(6)$$

Equation 6 consists of three subcomponents: α_j representing social interaction, β_j denoting the gravitational force on the ith grasshopper, and γ_j representing advection by wind. Social interaction, primarily driven by the grasshoppers themselves, is the predominant component, as shown in equation 7.

$$\alpha_i = \sum^{N}_{(j=1,\, k\neq j)} s(d_{jk})\,(\tilde{d}_{jk}) \quad ....(7)$$

where N represents the number of grasshoppers, $d_{jk}=|X_k-X_j|$ specifies the Euclidean distance between the j-th and the k-th grasshopper. $\tilde{d}_{jk}=(X_k-X_j)d_{jk}$ is a unit vector directed from the j-th grasshopper to the k-th grasshopper, and s is a function to define the strength of social forces represented by equation 8.

$$s(r) = fe^{-r/l} - e^{-r} \quad ....(8)$$

In this context, f represents the strength of attraction, r signifies the repulsive force, and l denote attractive length scale, which typically ranges from 0 to 4, regulating the balance between attraction and repulsion among grasshoppers. Regions devoid of both attraction and repulsion are termed as comfort zones, precisely positioned at a distance of 2.079. Normalization of distances to the interval [1, 4] is necessary since the function 's' cannot handle strong forces with large distances (Sajjad *et al.,* 2023). The β component has two parts, $\hat{g}$ is the gravitational constant and g shows a unity vector towards the center of earth. Mathematical definition is given in equation 9.

$$\beta_j = -g\hat{g} \quad ....(9)$$

The advection of the wind y_i is represented by equation 10:

$$\gamma_j = u\hat{w} \quad ....(10)$$

where u stands for the drift constant and $\hat{w}$ represents a unit vector in the direction of the wind. Using the components, we can write equation 6 as:

$$X_j = \sum^{N}_{k=1,\, k\neq j} s(|x_k - x_j|)\ ^{(Xk-Xj)/djk} - g\hat{g} + u\hat{w} \quad ....(11)$$

To solve optimization problems, a stochastic algorithm must effectively balance exploration and exploitation to accurately approximate the global optimum. The mathematical equation presented in 11 has included specific parameters to demonstrate exploration and exploitation at different stages of optimization. The mathematical equation is shown in equation 12.

$$X_j^d = c(\sum^{N}_{(k=1,\, k\neq j)} c\,((u_{bd} - l_{bd})/2)s(|x_k^d - x_j^d|)\,(X_k - X_j)/d_{jk}) + \tilde{T}_d \quad ....(12)$$

Where U_{bd} represents the upper limit and , L_{bd} denotes the lower limit in the d-th dimension, and $\tilde{T}_d$ represents the best solution found so far in the dth dimension space. The gravitational component G is disregarded, assuming no gravitational force, and the direction of the wind always points towards a target. The decreasing coefficient 'c' is utilized twice in equation 12 to regulate the forces among grasshoppers and is regenerated using equation 13. The outer 'c' maintains a balance between exploitation and exploration, while the inner 'c' diminishes repulsion or attraction forces among grasshoppers in proportion to

the maximum iteration count (Abualigah & Diabat, 2020).

$c = c_{max} - l\,(c_{max} - c_{min})/L$ ....(13)

where c_{max} represents the highest attainable value, while c_{min} stands for the lowest possible value. The variable l represents the ongoing iteration, and L signifies the maximum allowed iteration.

MATERIALS AND METHODS

The Test System

The aim of this study is to assess the effect GOA-tuned CSC-SMES unit in improving voltage profile and minimize real and reactive power losses on the IEEE 33-node distribution network with embedded WECS. Furthermore, the paper aims to compare the results obtained using GOA to tune the proposed CSC-SMES PI controller and that of a conventional PI controller. The various devices of the test system are briefly described as follows:

IEEE 33-Node Distribution Network

The Single Line Diagram (SLD) of the IEEE 33-nodes distribution network is shown in Figure 1. It comprises of thirty three node points and thirty two lines, with an embedded WECS integrated at node 22.

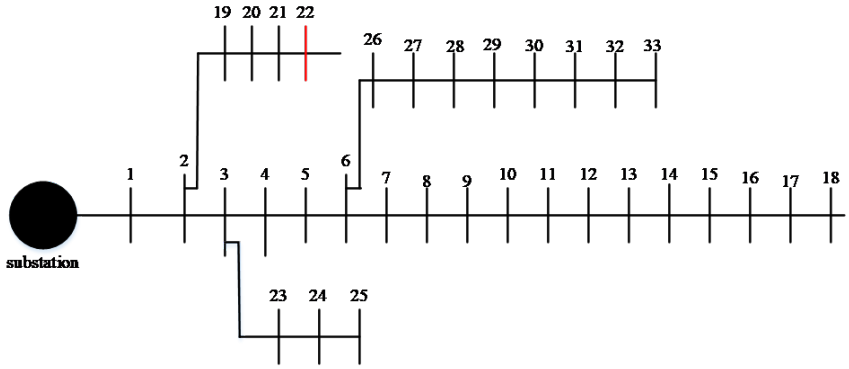

Figure 1: IEEE 33-Node Distribution Network's SLD

Wind Energy Conversion System

The Double Fed Induction Generator (DFIG) WECS is used in this study. DFIG stands out as the preferred option among WECS because of its ability to function at adjustable speeds (Abad *et al.,* 2011). The expression doubly fed denotes that the voltage of the stator is generated sourced from the three-phase electrical grid, while the rotor voltage is generated by the buck-to-buck converter. Control of the DFIG, under normal or abnormal conditions, is maintained by controlling the buck-to-buck converters with conventional controllers, as explained in (Yenealem *et al.,* 2020; Abdalkareem Jasim *et al.,* 2022). Table 1 shows the parameter values for the DFIG WECS that was utilized in the model.

Table 1: DFIG WECS parameters

No	Parameters	Values
1	Rated apparent power (Pn)	1.1 MVA
2	Phase-to-phase voltage voltage (Vn)	567 V
3	Operating frequency (f)	50 Hz
4	Resistance in the stator (Rs)	1.40 Ω
5	Inductance of the stator (Ls)	0.08998 mH
6	Resistance in the rotor (Rr)	0.99 Ω
7	Rotor inductance (Lr)	0.08208 mH
8	Mutual inductance between stator and rotor	1.5266 mH
9	Number of pole pairs	3

The aerodynamic characteristics of a wind turbine may be explained by the widely recognized $\overline{P}_c\,(\overline{R}, \overline{S})$ curves (Shi *et al.,* 2008). Here, the power coefficient PC is influenced by both the tip-speed ratio, R and the blade pitch angle, S. Once the power coefficient P_C is defined, equation 14 is utilized to calculate the mechanical power Generated by the turbine from wind energy.

$\overline{P}m = 1/2\ \rho A V_1^3\ \overline{P}_c\,(\overline{R}, \overline{S})$ ....(14)

Where,

$\overline{P}_c\,(\overline{R}, \overline{S}) = 0.5176\,(116/\overline{R}_i - 0.4\beta - 5)\,e^{(-21/Ri)} + 0.0068\overline{R}\,(1/\overline{R}_i)$ ....(15)

Superconducting Magnetic Energy Storage Unit and its Controller

The CSC controlled SMES has been used in this work due to its straightforward design, faster response

time, lower cost, and simpler control. The structure of the CSC-SMES is shown in Figure 2, consisting of a superconducting coil, two sets of 6-pulse ac/dc thyristor bridge converter, a three-winding transformer, a 12-pulse generator, a controller, filters and refrigeration components (Xing *et al.,* 2016). Two sets of 6-pulse bridge converters are employed to improve power factors, decreasing total harmonic distortion and the level of reactive power usage and increasing system reliability.

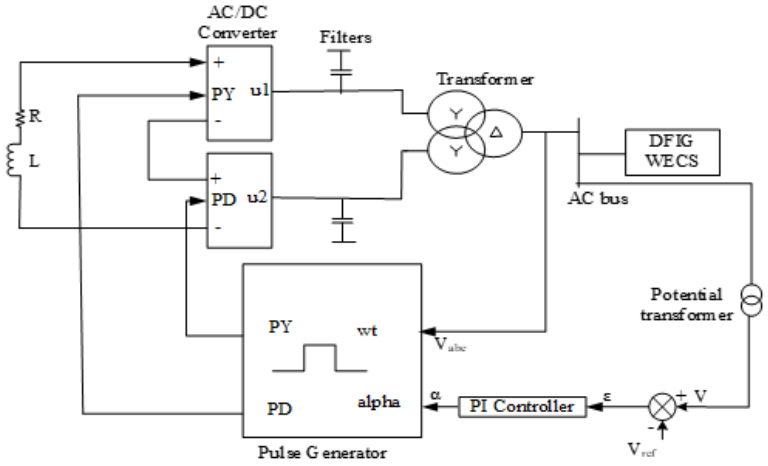

Figure 2: CSC-SMES block diagram

The management of the SMES is simplified by regulating the delay angle (α) of the 12-pulse generator. This action ensures the generation of accurate gate control signals, effectively controlling the successive firing of thyristors. When the angle α exceeds 90°, the converter operates as an inverter, allowing the SMES to release power to the coupling node. Conversely, if the angle α is less than 90°, the converter functions as a rectifier, enabling the SMES to absorb power from the distribution network (Xing *et al.,* 2016). Inductor coil (L) is used to represent a superconducting coil in this work. The energy stored in the SMES is calculated using equation 16. It parameters are given in Table 2.

$$E_{SMES} = 1/2\ LI^2 \quad ....(16)$$

Table 2: Parameters of the SMES

No.	Quantity	Values
1	Energy	1MJ
2	Current	1000A
3	Inductance	2.0 H

The universal bridge block in SIMULINK is used to implement a six-pulse bridge converter which can be obtained by connecting in series on the DC side and in parallel on the AC side two three-pulse converters. The bridge converter's output voltage results from combining the voltages of two converters algebraically. In the positive group, where there's a common cathode connection, the thyristor with the highest positive anode voltage conducts. Conversely, in the negative group with a common anode connection, when the cathode voltage is at its highest level, the thyristor conducts. Consequently, the voltage at the DC terminals for the output consists of portions of voltages in three phases. Commutations take place alternately between the positive and negative groups, ensuring that at any given time, two thyristors, one from the positive group and one from the negative group, are active. As the firing angle reaches 90°, the average DC voltage drops to zero, indicating power flow from AC to DC and the converter operates in rectifying mode. Continuing to increase the angle to 180° causes the mean voltage to rise from zero to its peak value with the polarity inverted. The converter functions in an inversion mode. However, it's important to note the existence of an inverter constraints, symbolized by the maximum firing angle (< 180°), above which the converter may experience commutation failure.

The Pulse Generator (Thyristor) block produces two pulse train sets to control a twelve-pulse thyristor converter, consisting of two three-phase Graetz bridges. In steady state, each pulse train has six evenly spaced square pulses, with a 90° phase shift between them. The PY pulses drive the six pulse bridge connected to the star (Y) secondary winding of the Y/Y/Δ transformer, while the PD pulses control the bridge linked to the secondary delta winding, with a 30° lead or lag optimization based on the delta configuration. The block is regulated by the alpha angle reference and a synchronization signal (wt), ranging from 0° to 180°, aligned with the zero crossings of the fundamental phase A voltage via a Phase Locked Loop (PLL). Internal wt ramps govern pulse timing, with the alpha delay angle determining the pulse delay relative to the commutating voltage's zero angle.

The PI controller is designed taken into consideration the compensation required by the test system and neglecting the internal loss of converters since optimal control of the PI controller can account for those losses. It features a simple structure, good stability, and robust resilience (Handayani *et al.,* 2020; Ali *et al.,* 2008). Its transfer function is represented by equation 17.

$$y(t) = K_p\ [\varepsilon(t) + 1/K_i \int_o^{\sigma} \varepsilon(t)dt] \quad ....(17)$$

The PI controller functions include:
The proportional term Kp contributes to the overall action and is directly proportional to the error signal.
The integral term Ki diminishes steady-state errors by implementing low-voltage compensation.
The GOA operates with a designated objective function to achieve the optimal value. Through this process, it determines the most optimal parameters for the SMES PI controller. The optimal configuration will yield a system that features an enhanced voltage profile with minimal active and reactive power losses. The assessment is conducted by computing the objective function value based on the network's response. In this work, the objective function employed is the Integral Time Absolute Error (ITAE) shown in equation 18. This objective function is appropriate for applications that require fast reaction and settling time.

$$ITAE = \int_0^{\infty} t|y(t)dt| \quad ....(18)$$

where yt represents the error signal between the reference and node voltages. The optimization problem is subject to the voltage constraint. The block diagram of the SMES PI controller scheme is shown in Figure 3.

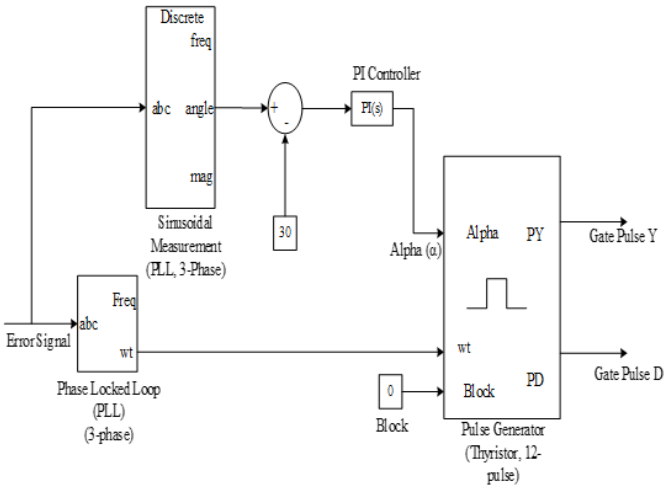

Figure 3: Block diagram of the SMES PI controller

The Procedure for GOA Tuning of SMES PI Controller
The flowchart shown in Figure 4 explained the steps of the applied GOA algorithm used in tuning the SMES PI controller.

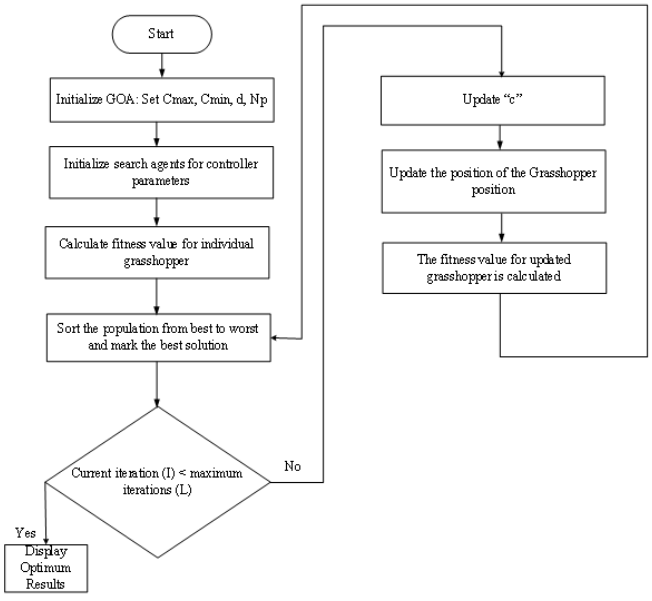

Figure 4: Flowchart of the GOA for tuning the SMES PI controller

Step 1: Initialize GOA parameters, along with the population size of grasshoppers, maximum iterations, minimum and maximum values of "c," lower and upper bounds, and the dimension, as specified in Table 3 and initialize the controllers' search agents.

Step 2: Population fitness is assessed using equation 18 by sorting from best to worst, and the best solution is identified.

Step 3: Check if the current iteration is less than the maximum; if yes, display the optimal results; if no, update

Table 3: GOA parameters

Setting	Symbol	Value
Population size of grasshoppers	$N^{\cdot}$	50
Maximum iteration count	L	100
Minimum c value	C_{min}	0.00004
Maximum c value	C_{max}	0.1
Lower limit	L_1	1
Upper limit	U_1	4
Problem dimension	d	2

the value using equation 13.

Step 4: Use equation 12 to update the existing search agents' positions, calculate the fitness of the updated search agents, and repeat Step 2.

Modelling and Simulation Procedures of the Test Systems

The IEEE 33-node distribution system, proposed SMES components and its GOA tuned PI controller and DFIG WECS are modelled in the SIMULINK environment. The modelling and simulation procedure of the test systems are as follows (Gade & Kotapuri, 2018):

i. Use the SLD of the IEEE, 33-node distribution test systems with the provided data for simulink modelling.

ii. Select, drag and place necessary components from the Simscape library, including distribution lines, generations sources, transformers, and loads.

iii. Connect the components according to the power system diagram and input the necessary technical data into the components.

iv. Save the Simulink file, execute the simulations to acquire voltage, active power, and reactive power values, and document the obtained outcomes.

v. Connect the modelled DFIG WECS block to the pre-selected node, save the simulink file, run the simulation to obtain and record the voltages, real and reactive powers

vi. Connect the SMES model with conventional PI controllers at the specified node, save the file and run simulation under increase in load conditions, obtain the voltages, real and reactive power and also the injected real and reactive by the SMES.

vii. Linked the designed GOA tuned controller to the SMES model, saved the files, run simulation under load increase conditions, obtained and records the same quantities as in step (vi).

RESULTS AND DISCUSSIONS

To assess the GOA tuned SMES PI controller for the improvement VPII and minimization of real and reactive power losses, the test systems were independently subjected to increase load demands by 5%, 10% and 15% respectively under state of discharge to evaluate the effect of load increments on the SMES PI controllers. The PI parameters, VPII and the real and reactive power losses, real and reactive power injected by the SMES are presented and discussed for the IEEE 33-node distribution test system. The real and reactive power was injected to satisfy the load demand using a controller, with a Kp value of 1.47 and Ki values of 0.76 for the conventional controller, and a Kp value of 1.66 and Ki values of 0.95 for the GOA tuned SMES controller.

In comparison to the conventional PI controller, the GOA-tuned superconducting magnetic energy storage (SMES) controller yielded substantial increases in real and reactive power injections across varying load demand increments. The real and reactive power injected are summarized in Table 4.

Table 4: Real and reactive power injected by the SMES controllers

Load Demand Increase	Active Power Injection Increase (%)	Active Power (p.u.) – Conv./GOA	Reactive Power Injection Increase (%)	Reactive Power (p.u.) – Conv./GOA
5%	7.01	0.456 / 0.488	30.43	0.023 / 0.030
10%	1.28	0.538 / 0.545	50.00	0.026 / 0.039
15%	2.19	0.684 / 0.699	54.84	0.031 / 0.048

The GOA-tuned SMES controller outperformed the conventional PI controller, achieving increased active power injection by 7.01% (from 0.456 p.u to 0.488 p.u) for a 5% load demand increase, 1.28% (from 0.538 p.u to 0.545 p.u) for a 10% load demand increase, and 2.19% (from 0.684 p.u to 0.699 p.u) for a 15% load demand increase. Similarly, reactive power injection improved by 30.43% (from 0.023 p.u to 0.030 p.u), 50.00% (from 0.026 p.u to 0.039 p.u), and 54.84% (from 0.031 p.u to 0.048 p.u) for 5%, 10%, and 15% load demand increases, respectively. These outcomes highlight the GOA-tuned SMES controller's superior capability in augmenting power injections to support system stability under dynamic load conditions.

The test system's VPII was 0.954, which is below 1.0, indicating that the embedded DFIG WECS decreased the system's voltage magnitudes which constituted of 30% of the load demand. The GOA - tuned SMES controller demonstrated improvements in the VPII relative to the conventional PI controller under increase in load demands. The VPIIs' improvements are detailed in Table 5.

Table 5: VPII Improvement for the SMES controllers

Load Demand Increase	VPII Improvement (%)	VPII – Conv./GOA
5%	0.19	1.017 / 1.019
10%	0.19	1.014 / 1.016
15%	0.20	1.011 / 1.013

The GOA-tuned SMES controller enhanced the VPII by 0.19% (from 1.017 to 1.019) for a 5% load increase, 0.19% (from 1.014 to 1.016) for a 10% load increase, and 0.20% (from 1.011 to 1.013) for a 15% load increase.

This clearly shows that the GOA tuned SMES PI controller outperformed the conventional SMES PI controller in improving the VPII. Therefore, it can be concluded that GOA-tuned SMES controller effectively improved the VPII when compared to the conventional PI controlled SMES.

In comparison with the conventional PI controller, GOA-tuned SMES controllers achieved notable reductions in real and reactive power losses across varying load demand increments. The Real and reactive power loss minimization are summarized in Table 6.

Table 6: Real and reactive power losses reduction for the SMES controllers

Load Demand Increase	Real Power Loss Reduction (%)	Real Power Loss (p.u.) Conv./GOA	Reactive Power Loss Reduction (%)	Reactive Power Loss (p.u.) Conv./GOA
5%	1.35	0.222 / 0.219	3.32	0.211 / 0.204
10%	1.29	0.231 / 0.228	3.17	0.221 / 0.214
15%	2.15	0.264 / 0.257	4.16	0.240 / 0.230

For a 5% increase in load demand, real power losses were reduced by 1.35%, dropping from 0.222 p.u to 0.219 p.u. Similarly, a 10% load demand increase resulted in a 1.29% reduction in real power losses, from 0.231 p.u to 0.228 p.u, while a 15% increase achieved a 2.15% reduction, from 0.264 p.u to 0.257 p.u. Reactive power losses also saw significant improvements. With a 5% load demand increase, losses decreased by 3.32%, from 0.211 p.u to 0.204 p.u. For a 10% load demand increase, the reduction was 3.17%, from 0.221 p.u to 0.214 p.u, and for a 15% increase, losses dropped by 4.16%, from 0.240 p.u to 0.230 p.u. These results underscore the enhanced efficacy of the GOA-tuned SMES approach in mitigating power losses under dynamic load conditions.

CONCLUSION

In this study, the GOA was employed to optimally tune the SMES controller for improving the VPII and minimizing both real and reactive power losses within the test setup. The results demonstrate that the GOA-tuned SMES controller significantly improves VPII and achieves more minimizations in real and reactive power losses. Comparative analysis with conventional SMES controllers confirms the exceptional performance of the GOA-tuned SMES controllers in enhancing system stability and efficiency. Overall, the integration of a GOA-tuned SMES controllers offers a promising solution for improving power system performance. Future work may focus on exploring other recent metaheuristic algorithms for CSC-SMES PI controller optimization, particularly in large-scale networks.

REFERENCES

Abad, G., Lopez, J., Rodrıguez, M., Marroyo, L., & Iwanski, G. (2011). *Doubly fed induction modeling and control.* 633.

Abdalkareem Jasim, S., Mireya Romero Parra, R., Salam Karim, Y., Mahdi, A. B., Jade Catalan Opulencia, M., Fakhriddinovich Uktamov, K., & Thaeer Hammid, A. (2022). Optimization of doubly-fed induction generator (DFIG) based wind turbine to achieve maximum power generation with imperialist competitive algorithm (ICA). *Science Progress, 105*(3). https://doi.org/10.1177/00368504221113193

Abdelbadie, H. T., Taha, A. T., Hasanien, H. M., Turky, R. A., & Muyeen, S. M. (2022). Stability enhancement of wind energy conversion systems based on optimal superconducting magnetic energy storage systems using the Archimedes optimization algorithm. *Processes, 10*(2), 366. https://doi.org/10.3390/pr10020366

Abualigah, L., & Diabat, A. (2020). A comprehensive survey of the Grasshopper optimization algorithm: results, variants, and applications. *Neural Computing and Applications, 32*(19), 15533–15556. https://doi.org/10.1007/s00521-020-04789-8

Adetokun, B. B., Oghorada, O., & Abubakar, S. J. afar. (2022). Superconducting magnetic energy storage systems: Prospects and challenges for renewable energy applications. *Journal of Energy Storage, 55*(PC), 105663. https://doi.org/10.1016/j.est.2022.105663

Ali, M. H., Murata, T., & Tamura, J. (2008). Transient stability enhancement by fuzzy logic-controlled SMES considering coordination with optimal reclosing of circuit breakers. *IEEE Transactions on Power Systems, 23*(2), 631–640. https://doi.org/10.1109/TPWRS.2008.920045

Aly, M. M., Salama, H. S., & Abdel-Akher, M. (2017).

Power control of fluctuating wind/PV generations in an isolated Microgrid based on superconducting magnetic energy storage. 2016 *18th International Middle-East Power Systems Conference, MEPCON 2016 - Proceedings, 1*, 419–424. https://doi.org/10.1109/MEPCON.2016.7836925

Borozan, V., Baran, M. E., & Novosel, D. (2001). Integrated Volt/Var control in distribution systems. *Proceedings of the IEEE Power Engineering Society Transmission and Distribution Conference, 3*(WINTER MEETING), 1485–1490. https://doi.org/10.1109/pesw.2001.917328

Buckles, W., & Hassenzahl, W. V. (2000). Superconducting magnetic energy storage. *IEEE Power Engineering Review, 20*(5), 16–20. https://doi.org/10.1109/39.841345

Burke, M. J., & Stephens, J. C. (2018). Political power and renewable energy futures: A critical review. *Energy Research and Social Science, 35*(November), 78–93. https://doi.org/10.1016/j.erss.2017.10.018

Calderaro, V., Conio, G., Galdi, V., Massa, G., & Piccolo, A. (2014). Optimal decentralized voltage control for distribution systems with inverter-based distributed generators. *IEEE Transactions on Power Systems, 29*(1), 230–241. https://doi.org/10.1109/TPWRS.2013.2280276

Chaychizadeh, F., Dehghandorost, H., Aliabadi, A., & Taklifi, A. (2018). Stochastic dynamic simulation of a novel hybrid thermal-compressed carbon dioxide energy storage system (T-CCES) integrated with a wind farm. *Energy Conversion and Management, 166*, 500–511. https://doi.org/10.1016/J.ENCONMAN.2018.04.050

El Moursi, M. S., Zeineldin, H. H., Kirtley, J. L., & Alobeidli, K. (2014). A dynamic master/slave reactive power-management scheme for smart grids with distributed generation. *IEEE Transactions on Power Delivery, 29*(3), 1157–1167. https://doi.org/10.1109/TPWRD.2013.2294793

Gade, V. C., & Kotapuri, M. R. (2018). A Three Phase Matlab Simulink Model of IEEE 57 Bus Power System Network. *International Journal of Engineering & Technology, 7*(4.24), 142. https://doi.org/10.14419/ijet.v7i4.24.21875

Handayani, L., Abu-Siada, A., Suwarno, S., Hariyanto, N., & Djalal, M. R. (2020). Power system performance enhancement using superconducting magnetic energy storage unit and proportional integral derivative control. 2020 *2nd International Conference on Smart Power and Internet Energy Systems, SPIES 2020*, 281–286. https://doi.org/10.1109/SPIES48661.2020.9242922

Haque, M. T., & Najafi, S. (2005). Application of neuro-fuzzy dynamic programming to improve the reactive power and voltage profile of a distribution substation. *Proceedings - Wec 05: Fourth World Enformatika Conference, 6*(6), 126–129.

Hasanien, H. M., & Muyeen, S. M. (2015). Particle swarm optimization-based superconducting magnetic energy storage for low-voltage ride-through capability enhancement in wind energy conversion system. *Electric Power Components and Systems, 43*(11), 1278–1288. https://doi.org/10.1080/15325008.2015.1027017

Kumar, P. P., Nuvvula, R. S. S., & Manoj, V. (2022). Grass Hopper Optimization Algorithm for Off-Grid Rural Electrification of an Integrated Renewable Energy System. *E3S Web of Conferences, 350*, 02008. https://doi.org/10.1051/e3sconf/202235002008

Liu, F., Mei, S., Xia, D., Ma, Y., Jiang, X., & Lu, Q. (2004). Experimental evaluation of nonlinear robust control for SMES to improve the transient stability of power systems. *IEEE Transactions on Energy Conversion, 19*(4), 774–782. https://doi.org/10.1109/TEC.2004.827703

Luo, Wang, J., & Krupke, C. (2014). Overview of Current Development in Compressed Air Energy Storage Technology. *Energy Procedia, 62*, 603–611. https://doi.org/10.1016/j.egypro.2014.12.423

Mahlia, T. M. I., Saktisahdan, T. J., Jannifar, A., Hasan, M. H., & Matseelar, H. S. C. (2014). A review of available methods and development on energy storage; Technology update. *Renewable and Sustainable Energy Reviews, 33*(May), 532–545. https://doi.org/10.1016/j.rser.2014.01.068

Meraihi, Y., Gabis, A. B., Mirjalili, S., & Ramdane-Cherif, A. (2021). Grasshopper optimization algorithm: Theory, variants, and applications. *IEEE Access, 9*, 50001–50024. https://doi.org/10.1109/ACCESS.2021.3067597

Mirjalili, S. Z., Mirjalili, S., Saremi, S., Faris, H., & Aljarah, I. (2018). Grasshopper optimization algorithm for multi-objective optimization problems. *Applied Intelligence, 48*(4), 805–820. https://doi.org/10.1007/s10489-017-1019-8

Muisyo, I. N., Muriithi, C. M., & Kamau, S. I. (2022). Enhancing low voltage ride through capability of grid connected DFIG based WECS using WCA-PSO tuned STATCOM controller. *Heliyon, 8*(8), e09999. https://doi.org/10.1016/j.heliyon.2022.e09999

Mukherjee, P., & Rao, V. V. (2019). Superconducting magnetic energy storage for stabilizing grid integrated with wind power generation systems. *Journal of Modern Power Systems and Clean Energy, 7*(2), 400–411. https://doi.org/10.1007/s40565-018-0460-y

Nielsen, K. E., & Molinas, M. (2010). Superconducting Magnetic Energy Storage (SMES) in power systems with renewable energy sources. *IEEE International Symposium on Industrial Electronics*, 2487–2492. https://doi.org/10.1109/ISIE.2010.5637892

Paserba, J., Electric, M., Products, P., & Miller, N. W. (2017). *Coordination of a distribution level continuously controlled compensation device with existing substation equipment for long term VAR management.* October. https://doi.org/10.1109/61.296288

Petropoulos, A. D., Koutsoukis, N. C., Karapidakis, E. S., & Georgilakis, P. S. (2014). Optimal mix of wind generation and energy storage systems

in power distribution networks. *IET Conference Publications, 2014*(CP665). https://doi.org/10.1049/CP.2014.1640

Qais, M. H., Hasanien, H. M., & Alghuwainem, S. (2020). Output power smoothing of wind power plants using self-tuned controlled SMES units. *Electric Power Systems Research, 178*(August 2019), 106056. https://doi.org/10.1016/j.epsr.2019.106056

Sadiq, R., Wang, Z., Chung, C. Y., Zhou, C., & Wang, C. (2021). A review of STATCOM control for stability enhancement of power systems with wind/PV penetration: Existing research and future scope. *International Transactions on Electrical Energy Systems, 31*(11), 1–27. https://doi.org/10.1002/2050-7038.13079

Said, S., Aly, M., & Hartmann, B. (2019). A robust SMES control for enhancing stability of distribution systems fed from intermittent wind power generation. *Turkish Journal of Electrical Engineering and Computer Sciences, 27*(5), 3883–3898. https://doi.org/10.3906/elk-1810-10

Said, S. M., Selim, A., & Hartmann, B. (2018). Enhancement of Voltage profile for Unbalanced Distribution System with Wind Energy and Superconducting Magnetic Energy Storage. 289–295.

Sajjad, F., Rashid, M., Zafar, A., Zafar, K., Fida, B., Arshad, A., Riaz, S., Dutta, A. K., & Rodrigues, J. J. P. C. (2023). An efficient hybrid approach for optimization using simulated annealing and grasshopper algorithm for IoT applications. *Discover Internet of Things, 3*(1). https://doi.org/10.1007/s43926-023-00036-3

Sannigrahi, S., Ghatak, S. R., Basu, D., & Acharjee, P. (2019). Optimal placement of DSTATCOM, DG and their performance analysis in deregulated power system. *International Journal of Power and Energy Conversion, 10*(1), 105–128. https://doi.org/10.1504/IJPEC.2019.096725

Saremi, S., Mirjalili, S., & Lewis, A. (2017). Grasshopper Optimisation Algorithm: Theory and application. *Advances in Engineering Software, 105*, 30–47. https://doi.org/10.1016/j.advengsoft.2017.01.004

Shi, J., Tang, Y. J., Ren, L., Li, J. D., & Chen, S. J. (2008). Application of SMES in wind farm to improve voltage stability. *Physica C: Superconductivity and Its Applications, 468*(15–20), 2100–2103. https://doi.org/10.1016/j.physc.2008.05.135

Su, C. L. (2010). Stochastic evaluation of voltages in distribution networks with distributed generation using detailed distribution operation models. *IEEE Transactions on Power Systems, 25*(2), 786–795. https://doi.org/10.1109/TPWRS.2009.2034968

Sulaeman, S., Alharbi, F. T., Benidris, M., & Mitra, J. (2017). A new method to evaluate the optimal penetration level of wind power. *2017 North American Power Symposium, NAPS 2017*. https://doi.org/10.1109/NAPS.2017.8107332

Wang, J., Fu, C., & Zhang, Y. (2008). SVC control system based on instantaneous reactive power theory and fuzzy PID. *IEEE Transactions on Industrial Electronics, 55*(4), 1658–1665. https://doi.org/10.1109/TIE.2007.911933

Wolpert, D. H., & Macready, W. G. (1997). No free lunch theorems for optimization. *IEEE Transactions on Evolutionary Computation, 1*(1), 67–82. https://doi.org/10.1109/4235.585893

Wong, L. A., Ramachandaramurthy, V. K., Taylor, P., Ekanayake, J. B., Walker, S. L., & Padmanaban, S. (2019). Review on the optimal placement, sizing and control of an energy storage system in the distribution network. *Journal of Energy Storage, 21*(June 2018), 489–504. https://doi.org/10.1016/j.est.2018.12.015

Xing, Y. Q., Jin, J. X., Wang, Y. L., Du, B. X., & Wang, S. C. (2016). An Electric Vehicle Charging System Using an SMES Implanted Smart Grid. *IEEE Transactions on Applied Superconductivity, 26*(7). https://doi.org/10.1109/TASC.2016.2602245

Yakout, A. H., Hasanien, H. M., & Kotb, H. (2021). Proton Exchange Membrane Fuel Cell Steady State Modeling Using Marine Predator Algorithm Optimizer. *Ain Shams Engineering Journal, 12*(4), 3765–3774. https://doi.org/10.1016/J.ASEJ.2021.04.014

Yenealem, M. G., Ngoo, L. M. H., Shiferaw, D., & Hinga, P. (2020). Management of voltage profile and power loss minimization in a grid-connected microgrid system using fuzzy-based STATCOM controller. *Journal of Electrical and Computer Engineering, 2020*. https://doi.org/10.1155/2020/2040139

Ziadi, Z., & Abdel-Akher, M. (2014). Voltage control of unbalanced distribution system with wind energy conversion system and high photovoltaic penetration. *Proceedings - ICPERE 2014: 2nd IEEE Conference on Power Engineering and Renewable Energy 2014,* 146–151. https://doi.org/10.1109/ICPERE.2014.7067194